Development and early life stress sensitivity of the rat cortical microstructural similarity network

Rachel L. Smith[a,b,1], Stephen J. Sawiak[c,d], Lena Dorfschmidt[a], Ethan G. Dutcher[e], Jolyon A. Jones[c,e], Joel D. Hahn[f], Olaf Sporns[g,h], Larry W. Swanson[f], Paul A. Taylor[i], Daniel R. Glen[i], Jeffrey W. Dalley[a,c,e], Francis J. McMahon[b], Armin Raznahan[b], Petra E. Vértes[a,2], Edward T. Bullmore[a,2]

a Department of Psychiatry, University of Cambridge, Cambridge, CB2 0SZ, UK
b Human Genetics Branch, National Institute of Mental Health, Bethesda, MD, USA 20892
c Behavioural and Clinical Neuroscience Institute, University of Cambridge, Downing Site, Cambridge, UK
d Department of Physiology, Development and Neuroscience, University of Cambridge, Cambridge, CB2 3EL, UK
e Department of Psychology, University of Cambridge, Cambridge, CB2 3EB, UK
f Department of Biological Sciences, University of Southern California, Los Angeles, CA, USA 90089
g Indiana University Network Science Institute, Indiana University, Bloomington, IN, USA 47405
h Department of Psychological and Brain Sciences, Indiana University, Bloomington, IN, USA 47405
i Scientific and Statistical Computing Core, National Institute of Mental Health, NIH, Bethesda, MD, USA 20892

1 To whom correspondence should be addressed: rachel.smith2@nih.gov
2 P.E.V. contributed equally to this work with E.T.B.

Author Contributions: Conceptualization, R.L.S., F.J.M., A.R., P.E.V., E.T.B.; methodology, R.L.S., S.J.S., E.G.D., J.W.D., P.E.V., E.T.B.; formal analysis, R.L.S.; investigation, S.J.S., E.G.D., J.A.J; data curation, R.L.S., S.J.S., L.D., E.G.D., J.A.J, P.A.T., D.R.G., J.W.D.; software implementation, R.L.S., S.J.S., L.D., P.A.T., D.R.G.; writing – original draft, R.L.S., F.J.M., A.R., P.E.V., E.T.B.; writing – review and editing, R.L.S., S.J.S., L.D., E.G.D., J.A.J., J.D.H., O.S., L.W.S., P.A.T., D.R.G., J.W.D., F.J.M., A.R., P.E.V., E.T.B.; visualization, R.L.S.; supervision, F.J.M., A.R., P.E.V., E.T.B.; project administration, J.W.D., P.E.V., E.T.B.

Keywords: connectome, architectome, micro-structural MRI, translational neuroscience, structural similarity

ABSTRACT

The rat offers a uniquely valuable animal model in neuroscience, but we currently lack an individual-level understanding of the in vivo rat brain network. Here, leveraging longitudinal measures of cortical magnetization transfer ratio (MTR) from in vivo neuroimaging between postnatal days 20 (weanling) and 290 (mid-adulthood), we design and implement a computational pipeline that captures the network of structural similarity (MIND, morphometric inverse divergence) between each of 53 distinct cortical areas. We first characterized the normative development of the network in a cohort of rats undergoing typical development (N=47), and then contrasted these findings with a cohort exposed to early life stress (ELS, N=40). MIND as a metric of cortical similarity and connectivity was validated by cortical cytoarchitectonics and axonal tract-tracing data. The normative rat MIND network had high between-study reliability and complex topological properties including a rich club. Similarity changed during post-natal and adolescent development, including a phase of fronto-hippocampal convergence, or increasing inter-areal similarity. An inverse process of increasing fronto-hippocampal dissimilarity was seen with post-adult aging. Exposure to ELS in the form of maternal separation appeared to accelerate the normative trajectory of brain development – highlighting embedding of stress in the dynamic rat brain network. Our work provides novel tools for systems-level study of the rat brain that can now be used to understand network-based underpinnings of complex lifespan behaviors and experimental manipulations that this model organism allows.

Significance Statement

Network models derived from neuroimaging have revolutionized our understanding of human brain development but need translation into animal models to interrogate their underlying mechanisms. Rats provide a valuable model due to their complex behaviors and biological similarities to humans; however, in vivo models of individual-level brain networks remain underdeveloped. In this study, we present a novel computational pipeline to construct such networks from in vivo rat structural neuroimaging data. Our findings highlight the dynamic development and experiential sensitivity of fronto-hippocampal systems in rats, offering a reference for cross-species comparisons and mechanistic insights into brain architecture. To support broader research efforts, we include an open release of code and data for rat MIND similarity network analysis.

INTRODUCTION

Network models of macroscale brain organization have significantly transformed our understanding of the brain (1–4). Recent advances in human structural neuroimaging have provided robust methods for constructing individual brain networks (3), including structural similarity analysis (5–7). This approach infers inter-areal similarity from magnetic resonance imaging (MRI)-derived morphometric features, with nodes representing cortical areas and edges reflecting the strength of correlation or divergence between pairwise vectors or distributions of features. For example, morphometric inverse divergence (MIND) estimates similarity as the Kullback-Liebler divergence between one or more MRI feature distributions measured at voxel- or vertex-level resolution (6). Evidence suggests that this macroscale MRI similarity reflects microscale cortical cyto- or myelo-architectonic similarity (6) and represents a broader principle wherein structurally similar regions tend to exhibit similarity across multiple phenotypic domains (8), including axonal inter-connectivity according to the homophily principle (6, 9). MIND networks and related methods have demonstrated high reproducibility (5, 6), developmental sensitivity (6, 10–15), environmental responsiveness (16–20), clinical relevance (21–28), significant heritability (6), and associations with gene expression (5, 6, 29). However, ethical constraints on human research highlight the critical role of animal models to disentangle the causal effects of environmental exposures on brain network development.

Rats are a widely used and valuable animal model in neuroscience due to their ease of use for high-throughput studies (unlike non-human primates) and their repertoire of complex behaviors that resemble those of humans (unlike mice) (30, 31). While mouse brain networks have been extensively characterized using imaging (32–41), tract-tracing (39, 42, 43) and spatial gene expression (44–47), comparatively little is known about network representations of the rat brain. Those data that do exist are primarily derived from expertly curated tract-tracing studies (4, 48–52) and suggest that the rat brain connectome exhibits complex topology (4) akin to that in humans (42, 53) and mice (42). However, these data represent the composite rat brain, limiting insights to group-level analyses and hindering the ability to explore individual variability. Developing an individual-level network model of the rat brain from a high-throughput, in vivo data modality would advance rat models for investigating the network underpinnings of brain development, behavior, and responses to experimental manipulations.

Given these considerations, we sought to advance the inter-species translation of techniques for MRI similarity analysis to represent the rat cortical network, and then leverage the experimental manipulability of the rat model to test for causal effects of early maternal separation on development of the rat cortical network. To achieve this goal, we harnessed two unique longitudinal neuroimaging datasets in rats (a normative developmental cohort and an experimental stress cohort; **Fig 1**; **Fig S1**) that measured magnetization transfer ratio (MTR), which is widely regarded as a proxy marker of cortical myelination (54–56). Myelination is an attractive feature in this context because it is known to be developmentally dynamic (57–59) and environmentally sensitive in rats (60–67), but has been underexplored in rat MRI studies using MTR (68).

We demonstrate that morphometric similarity defines a dynamic network architecture in the rat brain which can be validated against cytoarchitecture and axonal tract-tracing. Developmental findings reveal strengthening of fronto-hippocampal similarity alongside increased segregation of this system from other

brain regions - a process that declines in aging but is accelerated by exposure to early life stress. Our work provides novel tools for studying the systems-level organization of the rat brain that can be used to characterize network-level underpinnings of complex lifespan behaviors and experimental manipulations that this model organism allows. Code and data are available online as resources with this publication.

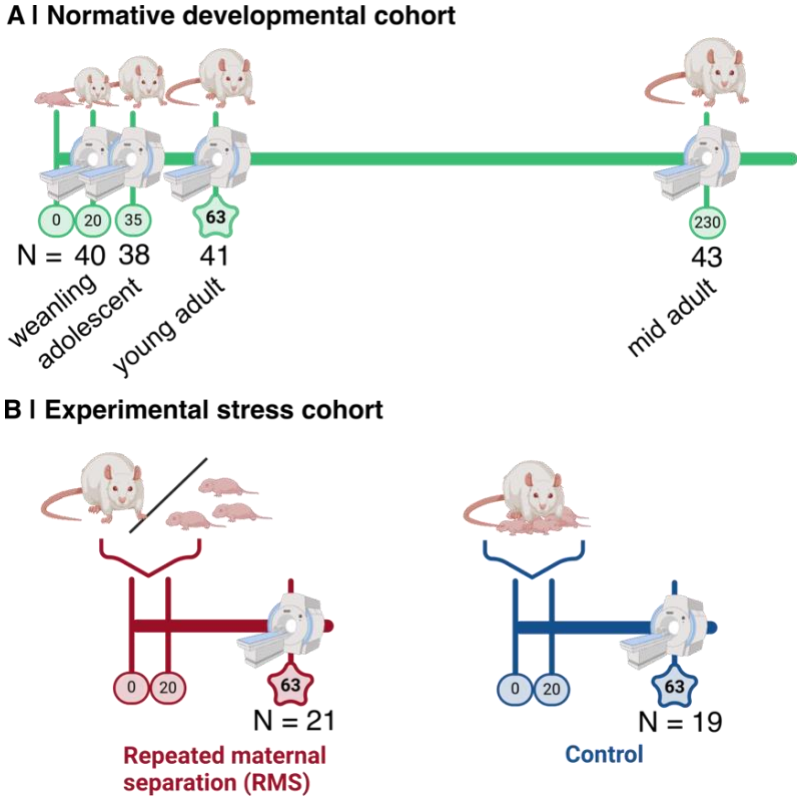

Figure 1. Two independent experimental cohorts to assess reliability and validity of rat MRI similarity networks as measures of developmental and stress-related changes in cortical microstructural networks. A) Study design for the normative developmental cohort: N=47 male Lister Hooded rats were reared normally and had brain MRI scanning at PND 20 (N=40), PND 35 (N=38), PND 63 (N=42), and within a few days of PND 230 (N=43). **B)** Study design for the experimental stress cohorts. N=21 Lister Hooded pups were stressed by repeated maternal separation (RMS), i.e., for 1 hour/day every day from PND 0 to PND 20, pre-weaning pups were separated from their dam. A control group of N=19 pups was reared normally. All animals completed MRI scanning at PND 63 as young adults. Figure created in https://BioRender.com.

RESULTS

Validation and reliability of the normative MIND microstructural network

We calculated each individual rat cortical network as the {53×53} matrix of edge weights (*w*) for all pairwise MIND similarity values between 53 areal nodes, and we estimated the normative cortical microstructural network as the median across edge weights in a sample of N=41 adult rat brains (postnatal day [PND] 63; young adulthood) from the normative cohort (**Fig 1A**; **Fig S1**; **Fig 2A**; **Fig S2**; **Table S2**). The 53 regions were grouped into 15 coarse-grained cortical systems, as defined by the Waxholm Space Atlas (71), for edge-level analyses and interpretability of results (**Fig 2B**; **Fig S3**).

The normative network distributions of nodal strength (i.e., the sum of all edge weights connecting it to the rest of the network, *s*) and edge weights were left-skewed (**Fig S4A** and **Fig S4B**, respectively; **Table S3**), indicating a generally high MTR-based anatomical similarity across the cortex. Hubs, defined as nodes with the highest strength (72), and rich-club organization, which examines whether hubs have stronger similarity with each other than expected by chance (73), are functionally relevant features of brain networks described in humans and other organisms (4, 42, 53, 74). We find this principle holds true in rat brain MIND networks. The hubs, defined as the 10 nodes with the highest strength, were largely hippocampal and piriform regions (**Fig 2C**; **Fig S5**). The rich club coefficient was 0.95, compared to a median coefficient of 0.45 across 10,000 distance-corrected null networks (**Fig S6**; **Fig S7**), indicating a significantly greater-than-random strength of connectivity amongst cortical hubs (Z=73; P < 0.001). This evidence for a rich club organization in MIND networks was consistent with prior reports of rich clubs in the meta-analytic connectome from rat tract-tracing data (4) and in other species and modalities of brain networks (74, 75).

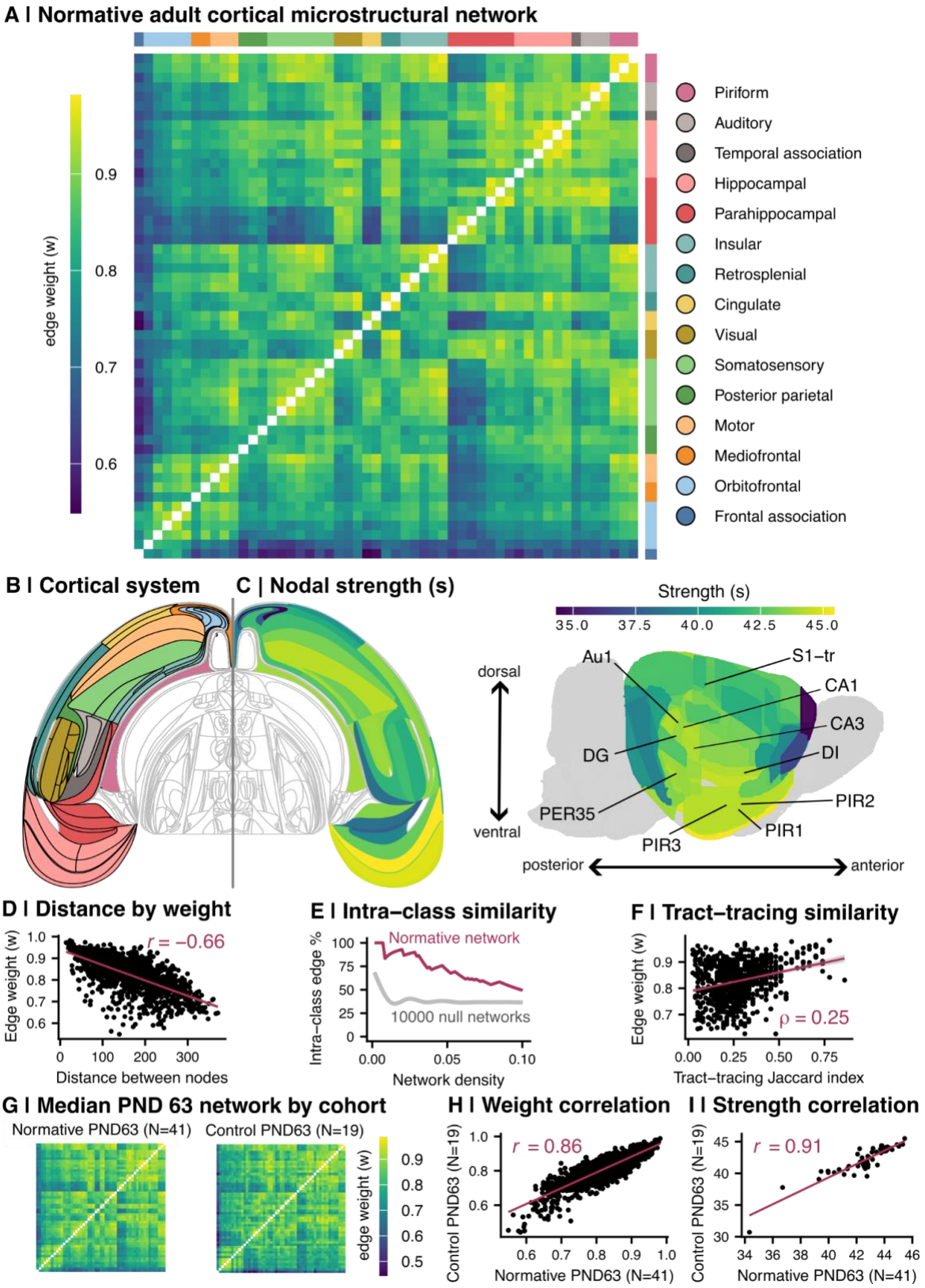
A | Normative adult cortical microstructural network
edge weight (w)
0.9
0.8
0.7
0.6
Piriform
Auditory
Temporal association
Hippocampal
Parahippocampal
Insular
Retrosplenial
Cingulate
Visual
Somatosensory
Posterior parietal
Motor
Mediofrontal
Orbitofrontal
Frontal association
B | Cortical system
C | Nodal strength (s)
Strength (s)
35.0 37.5 40.0 42.5 45.0
dorsal
ventral
Au1
S1–tr
CA1
CA3
DG
DI
PER35
PIR2
PIR1
PIR3
posterior
anterior
D | Distance by weight
Edge weight (w)
r = −0.66
Distance between nodes
E | Intra–class similarity
Intra–class edge %
Normative network
10000 null networks
Network density
F | Tract–tracing similarity
Edge weight (w)
ρ = 0.25
Tract–tracing Jaccard index
G | Median PND 63 network by cohort
Normative PND63 (N=41)
Control PND63 (N=19)
edge weight (w)
H | Weight correlation
r = 0.86
Control PND63 (N=19)
Normative PND63 (N=41)
I | Strength correlation
r = 0.91
Control PND63 (N=19)
Normative PND63 (N=41)

Figure 2. The normative rat cortical microstructural network: validation and reliability of MIND similarity networks. **A)** Heatmap representation of the normative rat connectome, defined as the median edge weight across rats in the normative cohort, at postnatal day 63 (PND63). Rows and columns are ordered by cortical systems, as indicated by annotation bars. Tile color indicates strength of MIND similarity (edge weight). **B)** A flatmap rendering of cortical systems (left hemisphere only) derived from (69, 70), color-coded as in (A). **C)** Maps of normative nodal strength. Left: Flatmap cortical rendering (right hemisphere only). Right: Anatomic MRI rendering. Network hubs, or top 10 nodes by strength, are labeled. CA1=cornu ammonis 1; PIR1=piriform cortex, layer 1; CA3=cornu ammonis 3; DG=dentate gyrus; S1-tr=primary somatosensory area, trunk representation; DI=dysgranular insular cortex; PIR2=piriform cortex, layer 2; PIR3=piriform cortex, layer 3; PER35=perirhinal area 35; Au1=primary auditory area. **D)** Scatterplot of the distance between two nodes (x-axis) and their MIND similarity, or edge-weight between them (y-axis). Distance is defined as the Euclidean distance between region of interest centers, as determined using the Waxholm Space atlas. **E)** Proportion of intra-class edges across network density thresholds. The x-axis shows the proportion of top-weighted edges considered, while the y-axis indicates the percentage of those top-weighted edges that consists of two regions from the same cortex class. The maroon curve shows the percentage of within-class edges in the normative MIND network, while the gray line shows the mean percentage (+/- sd) of within-class edges across 10000 permuted null networks. **F)** Correlation between similarity of tract-tracing connection profiles between pairwise combinations of regions and strength of MIND similarity. The Jaccard index for edge *ij* was defined as the intersection of tract-tracing connections (i.e., where *ik* == *jk*) divided by the union of all connections containing *i*, *j*, or both. In a null distribution of 10000 distance-corrected networks, normative network Spearman correlation Z=6; P < 0.001. **G)** Side-by-side heatmap comparison of the median PND 63 network from the normative developmental cohort (left; same as **Fig2A**) and the median PND 63 control network from the experimental stress cohort (right). The cophenetic correlation between the two networks is 0.55. Tile color indicates edge weight. **H)** The relationship between edge weights in the median PND 63 network from the normative development cohort (x-axis) and median PND 63 control network from the experimental stress cohort (y-axis; Pearson's r=0.86; P < 0.001). Each point represents an edge; the line of best fit is shown in maroon. **I)** The relationship between nodal strength in the median normative network (x-axis) and median control network from the stress cohort (y-axis; Pearson's r=0.91; P < 0.001). Each point represents a region of interest; the line of best fit is shown in maroon.

We validated the normative MIND network against four key predictions: that MIND similarity was greater between regions that (i) were spatially closer to each other, (ii) were more architectonically similar to each other, (iii) had more similar profiles of axonal projections in prior tract-tracing data, and (iv) had more similar gene expression profiles. All four of these predictions were verified as detailed below.

First, we found that morphometric similarity decreased with increasing distance between regions such that the Euclidean distance between node centers (calculated using Equation 2 in anatomical space) was negatively correlated with edge weight (r=-0.66; P < 0.001; **Fig 2D**).

Second, by co-registering our neuroimaging data with a cytoarchitectonic atlas of the rat brain (76), we found that MIND edges between regions within the same cortical type or class ("intra-class edges") had higher similarity than edges between cortical areas belonging to different classes ("inter-class edges"). Specifically, intra-class edges between two areas of allocortex had significantly higher similarity than edges between one allocortical ("allo") and one mesocortical ("meso") area (FDR < 0.05); however, meso intra-class edges were not significantly more similar than inter-class edges (**Fig S8**). To probe this relationship further, we calculated the percentage of intra-class edges (allo-allo and meso-meso) at various binary network densities (thresholded over a range of sparse connection densities from 1% to 10% of all possible pairwise edges) and compared this to the percentage of intra-class edges in distance-corrected null networks thresholded at the same range of connection densities (**Fig 2E**). Across all thresholds, the empirical rat network demonstrated a significantly higher percentage of intra-class edges than the null networks (**Fig 2E**), indicating a higher-than-chance density of cytoarchitectonically similar edges among edges with the highest MIND similarity.

Third, we converted meta-analytic rat tract-tracing data (4) to a similarity matrix by calculating the Jaccard index of the log10-transformed ordinal connection weight between pairwise regions (Equation 1; **Fig S9A**). This metric, representative of the similarity of axonal connection profiles, was positively correlated with edge weight (ρ=0.25; P < 0.001; **Fig 2G**). This relationship was significantly stronger than chance (Z=6.04 in distance-corrected null network distribution; P < 0.001).

Fourth, using homology between the rat and mouse brain to access spatially comprehensive transcriptomic data from the Allen Mouse Brain Atlas (46), we tested and verified that regions with higher MIND similarity also demonstrated higher transcriptomic similarity, calculated as the pairwise regional correlation between gene expression profiles (**Fig S10**).

Finally, to assess the reliability of MIND network analysis, we directly compared the median adult MIND network for the normative developmental cohort (N=41, PND 63) to the median adult MIND network for an independent cohort of rats: namely, the normally reared (control) group in the experimental stress cohort (N=19, PND 63) (**Fig 1B**; **Fig 2H**). Edge weights were highly correlated between the normative adult and independent control MIND networks (r=0.86; P < 0.001; **Fig 2I**), as was nodal strength (r=0.91; P < 0.001; **Fig 2J**). These results demonstrate a high level of replicability of the cortical microstructural network estimated by identically implemented MIND analyses of MTR data collected using the same sequences in two independent cohorts of rats.

Normative developmental changes in the rat cortical microstructural network

Having established convergent validity and inter-sample replicability of MIND networks, we next harnessed this analytic approach to model network level reorganization of the rat brain over development. This strategy, applied to a longitudinal MRI dataset spanning PND 20, 35, 63 and 230 (N=162 total scans, **Fig 1A**, **Methods**, **Table S1**), revealed developmental changes in (i) each region's morphometric similarity with the rest of the brain (strength, s), and (ii) the morphometric similarity (edge strength, w) between each unique pair of regions. Visual inspection of the median MIND matrices for each of the four time-points indicated that there are age-related changes in the cortical pattern of inter-areal similarity. For example, frontal cortical areas (frontal association cortex, orbitofrontal cortex, mediofrontal cortex, and motor areas) become more similar to the rest of the cortex during early development, and then strikingly less similar during later aging (**Fig 3A**). Likewise, nodal strength showed a general tendency to increase during development and decrease during aging (**Fig 3B**).

We quantified the regional rate of change in early development as the linear gradient or slope of age-related change in nodal strength for each cortical area between PND 20 (weanling) to PND 35 (adolescence), Δs_{dev}**,** accounting for inter-subject variation (Equation 2A; **Fig S11**). Similarly, to calculate changes in aging, we applied the same model to estimate the age-related change in strength for each cortical area from PND 63 (young adult) to PND 230 (mid adult) timepoints, Δs_{age}.

During development, regions in most cortical systems significantly increased in nodal strength, especially the hippocampal formation and motor cortex (Δs_{dev} t-values=7.19 and 5.22, respectively; **Fig 3C**). The parahippocampal region decreased in similarity with the rest of the brain (Δs_{dev} t=-1.34). In contrast to these developmental changes, most cortical systems decreased in nodal strength, especially areas of the frontal cortex, including the orbitofrontal (Δs_{age} t=-11.4), motor (Δs_{age} t=-6.13), and mediofrontal (Δs_{age} t=-5.94; **Fig 3D**) cortices. Early life and aging effects on nodal strength were negatively correlated (r=-0.39; P=0.004; **Fig 3E**), indicating that those regions showing the strongest strength increases in development also tended to show the most rapid strength decreases in aging. Ten fronto-hippocampal regions both significantly increased in strength in early development and significantly decreased in strength in aging (**Fig S12**). Only one region, the parasubiculum, significantly decreased in early development and increased in aging.

We also calculated changes in early development and aging for each inter-areal similarity or edge in the MIND networks (Δw_{dev} and Δw_{age}, respectively; Equation 2B). In early development, the hippocampal formation demonstrated notable increases in similarity with frontal regions, including the orbitofrontal (Δw_{dev} t=17.6), motor (Δw_{dev} t=15.5), frontal association (Δw_{dev} t=11.7), and mediofrontal (Δw_{dev} t=7.97) cortices (**Fig 3G**). In contrast, parahippocampal regions largely decreased in similarity with other cortical systems, including the somatosensory (Δw_{dev} t=-13.4) and piriform (Δw_{dev} t=-11.0) cortices. In aging, the most salient changes in edge weight involved orbitofrontal regions, which significantly diverged from every other cortical system, most notably the somatosensory (Δw_{age} t=-30.1), hippocampal (Δw_{age} t=25.7), parahippocampal (Δw_{age} t=22.5) regions (**Fig 3H**). As with strength, edge weight effects during development and aging were negatively correlated (r=-0.55; P < 0.001; **Fig 3F**), demonstrating that frontal and hippocampal systems with the most rapid increases in pairwise similarity during early development showed the fastest decreases in similarity, or increases in dissimilarity, during aging.

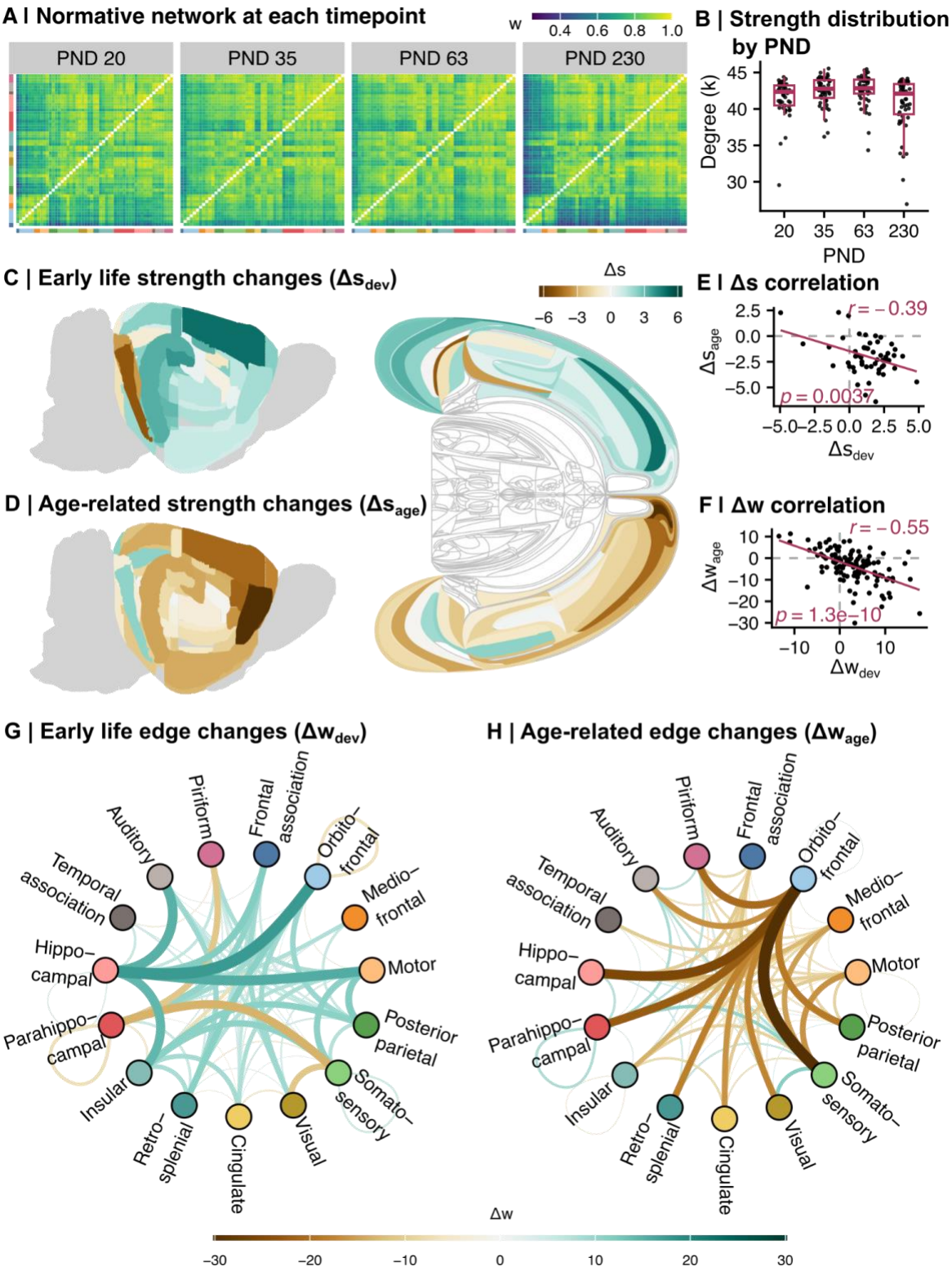
A | Normative network at each timepoint
w
0.4 0.6 0.8 1.0
PND 20
PND 35
PND 63
PND 230
B | Strength distribution by PND
Degree (k)
45
40
35
30
20 35 63 230
PND
C | Early life strength changes (Δs_dev)
Δs
−6 −3 0 3 6
D | Age-related strength changes (Δs_age)
E | Δs correlation
r = −0.39
p = 0.0037
Δs_age
Δs_dev
F | Δw correlation
r = −0.55
p = 1.3e−10
Δw_age
Δw_dev
G | Early life edge changes (Δw_dev)
H | Age-related edge changes (Δw_age)
Auditory
Piriform
Frontal association
Orbito-frontal
Medio-frontal
Temporal association
Hippo-campal
Motor
Parahippo-campal
Posterior parietal
Insular
Somato-sensory
Retro-splenial
Cingulate
Visual
Δw
−30 −20 −10 0 10 20 30

Figure 3. The normative rat cortical connectome generally increases in similarity in early development and decreases in similarity in aging. A) Heatmap representation of the connectome throughout development in the normative cohort (median edge weight, at each timepoint). Rows and columns are ordered by decreasing-to-increasing nodal strength within broader cortical system (in the same order as Fig 2A). Tile color indicates strength of MIND similarity (edge weight, w). **B)** The normative strength distribution through development, defined as the median strength per ROI at each timepoint. Each point represents a region of interest; boxplots show the overall strength (*s*) distribution at each timepoint. The normative strength distribution at PND 20 is significantly lower than the distribution at PND 63 (Dunn test P=0.019); the nodal strength distribution at PND 230 is significantly lower than the distributions at PND 35 (Dunn test P=0.027) and PND 63 (Dunn test P=0.003) (Krustal-Wallis P=0.002). **C)** Anatomical patterning of nodal strength changes in early development (Δs_{dev}). Left: Volumetric rendering; Right: Flatmap rendering (left hemisphere/top half only; (69, 70)). Brown indicates decrease in strength, teal indicates increase in strength. Δs_{dev} was considered significant if |*t*-value| of the age term in the mixed effects model was greater than 2. **D)** Anatomical patterning of nodal strength changes in aging (Δs_{age}; flatmap rendering right hemisphere/bottom half). Figure key same as Fig 3C. **E)** Pearson correlation between Δs_{dev} (x-axis) and Δs_{age} (y-axis; r=-0.39; P=0.004). Each point represents a region of interest; the line of best fit is shown in maroon. **F)** Pearson correlation between Δw_{dev} (x-axis) and Δw_{age} (y-axis; r=-0.55; P < 0.001). Each point represents an edge; the line of best fit is shown in maroon. **G)** A circle plot of significantly changed system-level edges in early development (Δw_{dev}; $|t|$> 3.3). Each datapoint in the circle represents a broader cortical system, colored and labeled by system. The color and size of the curves connecting two points show the change in edge weight (brown indicates decreasing similarity; teal indicates increasing similarity). **H)** A circle plot of significantly changed edges in aging (Δw_{age}). Figure key is the same as Fig 3G.

Early life environmental stressors perturb adult cortical similarity networks

We assessed the impact of early life stress - as modeled by repeated maternal separation (RMS) - on the nodal strength of the young adult cortical microstructural network by running multiple case-control comparisons for each cortical area at the PND 63 timepoint (Equation 3A; **Fig 1B**). Exposure to RMS was associated with strength decreases in most brain regions (N=40 of 53 total) (**Fig 4A**). Four regions had significant differences following permutation testing: the lateral entorhinal cortex, perirhinal area 36, and cingulate area 1 decreased in strength in RMS (permutation Z-scores=-3.07, -2.31, and -2.18, respectively), while the frontal association cortex demonstrated increased strength following RMS (Z_{perm}=2.08; **Fig 4B**).

Qualitatively, visual inspection of the median MIND matrices in control (N=19) and RMS-exposed rats (N=21) indicated that the early life stressor induced changes in the cortical pattern of inter-areal similarity, especially in frontal and hippocampal systems (**Fig 4C**). Indeed, edge-level case-control analyses (Equation 3B) showed that RMS-exposed rats had strongly decreased similarity between parahippocampal cortex and several other cortical areas (including the orbitofrontal cortex (t=-6.89), mediofrontal cortex (t=-5.89), and motor cortex (t=-4.69; **Fig 4D**). This contrasts with markedly increased similarity between the frontal association cortex and other areas, including the somatosensory (t=5.40) and insular cortices (t=5.17; **Fig 4D**). Together, these results indicate vulnerability in network structure to environmental stress, especially in frontal and parahippocampal regions most sensitive to developmental and aging changes in nodal strength.

Effects of early life stress are nested within normative developmental changes in the cortical microstructural network

Finally, we tested more formally for potential congruence between stress effects and normative network changes in development and aging. Strikingly, variation in the effects of RMS on inter-areal edge weights in the rat cortical microstructural network was positively correlated with variation in the edge weight changes over normative development (Δw_{dev}; r=0.18, P_{perm}=0.03; Z_{perm}=1.90; **Fig S13 (left)**). Specifically, those edges showing greatest similarity increases in normative development also tended to show greater similarity increases following RMS. Furthermore, the effects of RMS on edge weight were significantly and negatively correlated with normative age-related changes in edge weight (Δw_{dev}; r=-0.19, P_{perm}=0.02; Z_{perm}=-2.03; **Fig S13 (right)**), indicating that the edges with the greatest similarity increases following RMS were also those that decreased in similarity the most in normative aging. Taken together, these results are consistent with a model in which early life stress accelerated normative brain reorganization during development; and areas which are most developmentally dynamic and vulnerable to stress are also the most susceptible in aging.

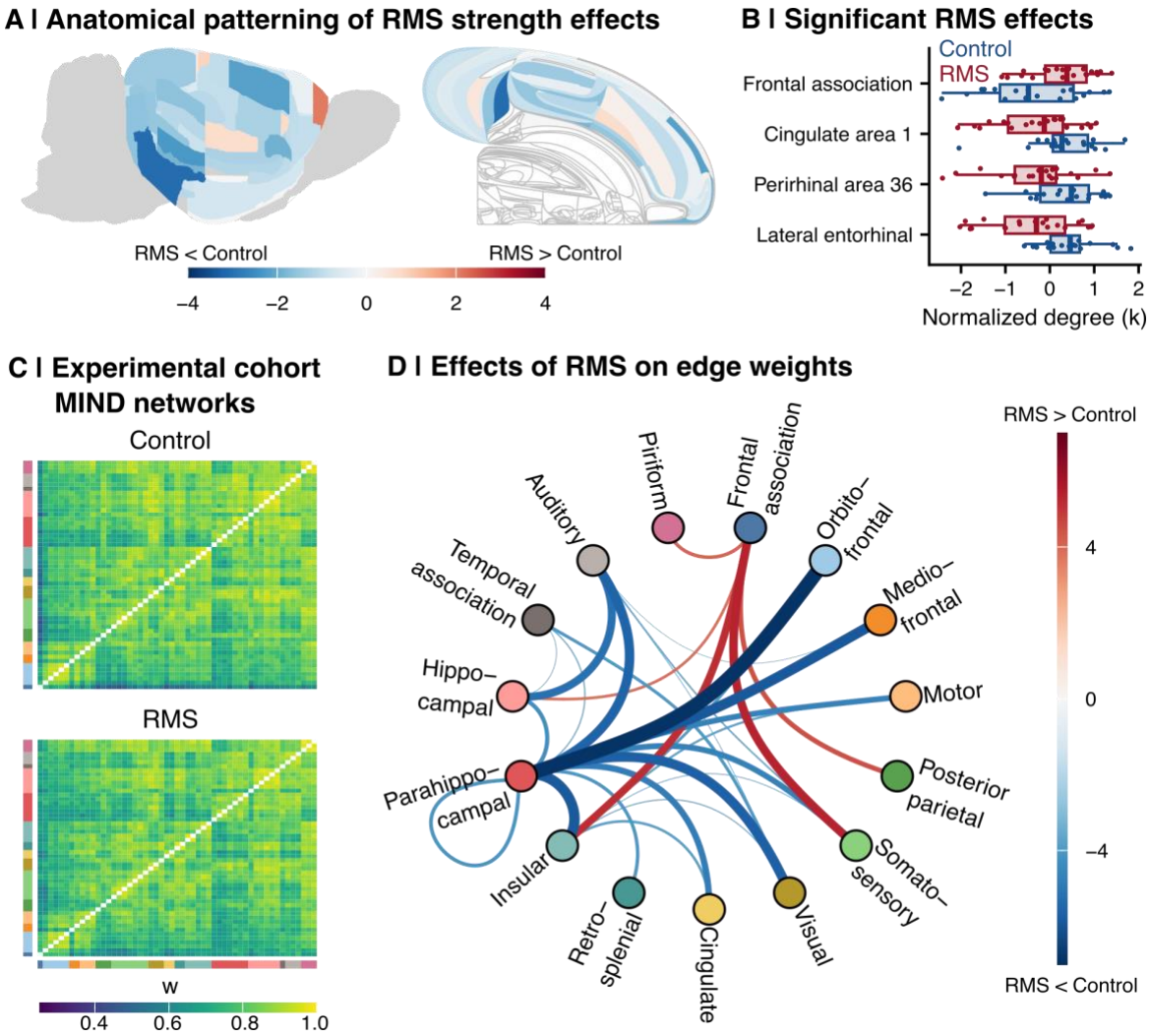

Figure 4. Impact of early life stress on nodal strength and edge weights. A) Anatomical distribution of the post-natal day 63 (young adulthood) RMS-control effect sizes across brain slices. For each region of interest, a linear model was run of the normalized strength on group + age + sex + TBV, and the group statistic was extracted as the actual effect size. Then, 1000 permutations were run in which the group assignments were shuffled, the same linear model was run, and the group statistic was extracted as the permuted effect size. The z-score of the actual effect size was calculated as its position in the permuted distribution. Regions with positive *Z*-scores (shown in red) demonstrated increased strength in RMS subjects in young adulthood; regions with negative *Z*-scores (shown in blue) demonstrated decreased strength. The flatmap rendering was derived from (69, 70). **B)** Boxplots showing the nodal strength distribution by group for the four regions with significant case-control differences at PND 63 ($|Z_{perm}| > 1.96$). The x-axis shows nodal strength, corrected for covariates and normalized for visualization purposes. Each point represents a subject, while the box-and-whiskers plot shows the overall distribution by group. Blue indicates control, red indicates RMS. **C)** The median PND 63 MIND networks in control subjects (top) vs RMS subjects (bottom). Figure legend is the same as **Fig 2A**. **D)** A circle plot of significant RMS-control edge weight differences in young adulthood (PND 63; $|t| > 3.3$). Node order and system annotation are the same as **Fig 3F** and **Fig 3G**. Curves connecting two points indicate a significant case-control difference in edge weight; colored by effect size (with red indicating higher weight in RMS and blue indicating higher weight in control); line width indicates absolute value effect size.

DISCUSSION

We have pioneered and validated MIND similarity network analysis as a novel approach to inferring myelo-architectonic similarity between all cortical areas in an individual rat's brain. Using this methodological advance, we studied N=47 rat cortical networks to investigate normative dynamics in cortical similarity

across development and aging. These changes, which primarily involved frontal and hippocampal systems, were examined through MIND analysis of myelin-sensitive MTR data collected up to four times over each rat's lifespan. In a second experiment, we tested the hypothesis that early life stress exposure was associated with subsequent abnormalities of cortical network organization. Repeated maternal separation in the first 20 days of postnatal life affected the adult similarity of cortical areas, especially frontal and hippocampal systems that are normatively most dynamic in adolescent development and early brain aging.

Structural MRI similarity analysis is being increasingly used as a measure of brain network organization in various methodological and experimental contexts (3). In general, the interpretation of MIND similarity rests on two key assumptions: (i) that the correlation or inverse divergence between MRI features in two cortical areas reflects their cyto-architectonic or myelo-architectonic similarity; and (ii) that cortical areas which are more architectonically similar are more likely to be axonally inter-connected (3, 8). We can therefore think of a structural MRI similarity network as primarily a map of cortical patterning – an architectome – which is in turn a partial proxy for the map of axonal wiring – a connectome. To validate rat brain MIND similarity analysis, we tested both these key assumptions. The results confirmed that cortical areas belonging to the same architectonic class, or spatially adjacent to each other, tended to have higher MIND similarity, and that higher MIND similarity between cortical areas was associated with stronger evidence of similarity in axonal connectivity, based on a prior meta-analysis of tract-tracing studies (4). Since the MRI data we used for this analysis were collected using a magnetization transfer (MTR) sequence that is known to be sensitive to cortical myelination and neuropil density (77), we can therefore generally interpret MTR-derived MIND (dis-)similarity as indicative of architectonic differentiation and myelination of the cortex of an individual rat.

To characterize the dynamics of such differentiation across the lifespan, we measured changes in similarity in early life, defined as PND 20 to 35, and in later life, defined as PND 63 to 230. Though the data on developmental patterns of rat brain myelination are sparse, a histological study demonstrated that the rat brain begins myelinating around PND 10, and most areas are fully myelinated by PND 24 (57). Thus, our "early" developmental data likely reflect the end of early life myelinating processes (e.g., late adolescence) and do not capture earlier peaks in cortical myelination. We show that increasing MIND similarity in fronto-hippocampal circuitry in late adolescent development ("early life") is coupled to rapidly decreasing similarity of these systems in mid-adulthood aging. These data thus support the "last in, first out" hypothesis of development and aging, in which plastic regions that mature last in early development (namely, frontal areas related to decision-making and executive function) are more vulnerable to age-related decline, as previously described in humans (78–80). We demonstrate here that rat brain microarchitecture is subject to the same phenomenon.

Developmentally sensitive fronto-(para)hippocampal circuitry also showed targeted disruptions in young adult rats who had been exposed to repeated maternal separation. This result aligns with studies in humans, in which later-developing plastic circuitry also shows increased vulnerability to disease processes in early development and aging, such as schizophrenia and Alzheimer's disease, respectively (78, 80). The congruence between developmentally dynamic and environmentally-sensitive regions was reinforced quantitatively, as edges that increased in similarity in development tended to show higher similarity following RMS (**Fig S13**). These results are consistent with an accelerated development hypothesis of early life stress (81). Edges that showed higher similarity in young adulthood following early life stress also demonstrated more rapid divergence in normative aging. This provides further support for the concept that specific fronto-hippocampal circuits are developmentally dynamic, vulnerable to age-related decline, and susceptible to environmental stress (78, 79).

An increase in similarity between two areas (in this case, frontal and hippocampal) does not necessarily indicate the formation of new axonal connections, but likely represents coordinated changes in (i) myelination of fibers, and/or (ii) microstructural properties, such as synaptic or dendritic remodeling. The first hypothesis is supported by rat histological data showing that, between PND 24 and PND 37, myelination occurs exclusively in the fornix and mammillothalamic tract—pathways that traverse the hippocampus (57). It has been argued theoretically that regions related to memory and learning develop as the adolescent rat ventures out and requires spatial recognition, a skill less essential earlier in life (57).

Consistent with this, a study on rat hippocampal myelination reported the first appearance of myelinated fibers at PND 17, a significant increase to near-adult levels by PND 25, and full maturation by PND 60 (82).

In addition to myelination, changes in MIND similarity may also arise from coordinated microstructural reorganization. Extensive cross-modality research highlights hippocampal plasticity in rodents, especially changes in synaptic density in response to environmental enrichment or deprivation (83–87). Similarly, the frontal cortex undergoes environmentally-sensitive synaptogenesis in early development - continuing into adulthood in rats (88) - and synaptic pruning throughout the lifespan (89). These shifting neuropil profiles suggest that cortical regions without direct physical connections may exhibit high MIND similarity due to convergent synaptic architectures—or increasingly divergent profiles with other regions. Our cross-validation data support this concept. In the tract-tracing (4) Jaccard comparison, a subset of edges showed low tract-tracing similarity but high MIND similarity, predominantly involving hippocampal regions. Excluding hippocampal edges strengthened the correlation between MIND similarity and tract-tracing ($\rho=0.41$; $P < 0.001$; **Fig S9B**). We postulate that the observed high MIND similarity, despite low axonal connection similarity, may reflect convergent plastic reorganization of the microstructural properties of these regions. Notably, the hypotheses of cortical fiber myelination and synaptic density as contributors to MIND similarity are likely interconnected, as evidence suggests neural activity can induce myelinogenesis (90).

Future work to characterize MRI-derived rat brain network architecture could include additional morphometric features, such as DTI metrics, in a multivariate MIND analysis. This could give a broader view of cortex-wide morphological co-variation and more directly represent axonal connections. As more rat brain resources become available (for instance, a brain-wide spatial transcriptomic atlas and consensus nomenclature/parcellations), this will enhance our ability to biologically annotate the rat structural similarity network. It would be of further interest to include developmentally and environmentally sensitive subcortical regions in future analyses, and, given adequate sample size, to interrogate sexual dimorphisms in network structure and dynamics.

We provide the normative MTR-derived rat cortical microstructural network as a resource to support further investigation and understanding of the complex organization of cortical networks in this key model system. Our results demonstrate the biological validity and replicability of the MIND similarity analysis and demonstrate its sensitivity to developmental and environmental stress-related changes in cortical network configuration. We emphasize the importance and vulnerability of key frontal and hippocampal circuitry in dynamic processes of normative development and atypical developmental trajectories triggered by early life adversity.

MATERIALS AND METHODS

Experimental design

Pre-existing structural MRI data from two independent cohorts were used to assess network-level changes that occur during development and in response to stress:

1. Normative development cohort (91) (**Fig 1A**)

Male Lister Hooded rats (N=47) were kept on a reverse light/dark cycle with red light on from 7:30am - 7:30pm and white light for the other half of the daily cycle. Rats underwent MRI scanning and weaning on postnatal day (PND) 20 or 21 (N=40; here referred to as PND 20). Rats were scanned again at PND 35 (N=38), PND 63 (N=42), and once between PND 212-244 (N=43; here referred to as PND 230). **Figure 1** shows the number of observations per animal in the normative developmental cohort, with 32 animals (68% of total) having scans at each of the four timepoints from PND 20 (post-weaning) to PND 230 (aging adult). Experiments were carried out in accordance with the (U.K Animals) Scientific Procedures Act (1986) under UK Home Office project licenses (PPL 70/7587 & PPL 70/8072) and were approved by the University of Cambridge Ethics Committee.

2. Experimental stress cohort (92) (**Fig 1B**)

Pregnant Lister Hooded rats (N=14) were purchased from Envigo (Blackthorn, UK). Litters were delivered by spontaneous partum on gestational days 22-24. Within three days of birth, litter size was adjusted to 4-6 pups, with each litter consisting of two female and two male pups (with the exception of one litter with four males and two females). If two litters were born within 24 hours of one another (the case for 10 litters in total), pups were mixed between the litters. After litter size adjustment, litters were allocated alternately by birth time to either the repeated maternal separation condition (RMS; N=30 pups: 14 female, 16 male) or the control condition (N=28 pups: 14 female, 14 male). PND 0 was defined as the day of delivery. Body weight was measured weekly starting at PND 20. Lights were on from 21:00 to 09:00. Experiments were conducted on Project License PA9FBFA9F, in accordance with the UK Animals (Scientific Procedures) Act 1986 Amendment Regulations 2012, the EU legislation on the protection of animals used for scientific purposes (Directive 2010/63/EU), and the GSK Policy on the Care, Welfare and Treatment of Animal, following ethical review by the University of Cambridge Animal Welfare and Ethical Review Body (AWERB).

From PND 5-19 (inclusive), pups from RMS litters were separated from their dam for 6 hours a day, starting between 11:00am-12:30pm. During separation, dams remained in their home cages while pups were taken to a different room and placed together inside a ventilated cabinet. One centimeter of bedding was provided and the temperature at the surface of the bedding was kept between 30 °C and 35 °C through warming of the air and use of an electric heat pad. Control pups were subject only to normal animal facility rearing. Following PND 20, pups from both groups were weaned and housed in same-sex pairs at PND 20 and left undisturbed until early adulthood except for weighing and once-weekly cage changes. All animals then underwent MRI scanning at PND 63.

MRI acquisition

For both cohorts, high-resolution MRI was performed on a 9.4T horizontal bore MRI system (Bruker BioSpec 94/20; Bruker Ltd.). Images were acquired under isoflurane anesthesia using the manufacturer-supplied rat brain array coil with the rat in a prone position. Structural images were obtained based on a 3D multi-gradient echo sequence (TR/TE 25/2.4 ms with 6 echo images spaced by 2.1 ms, flip angle 6° with RF spoiling of 117°). The field of view was 30.72 × 25.6 × 20.48 mm3 with a matrix of 192 × 160 × 160 yielding isotropic resolution of 160 µm with a total scan time of 6 min 36 sec with zero-filling acceleration (25% in the readout direction; 20% in each phase encoding direction). Magnetization transfer pulses (10 µT, 2 kHz off-resonance) were applied within each repetition to enhance gray-white matter contrast. Post-reconstruction, images from each echo were averaged after weighting each by its mean signal.

Throughout all scanning procedures, rats were anesthetized with isoflurane (1-2% in 1L/min O2: air 1:4). Respiratory rate, oxygen saturation and pulse rate (SA Instruments; Stony Brook, NY) were measured with anesthetic dose rates adjusted to ensure readings remained within a physiological range. Body temperature was measured and regulated with a rectal probe and heated water system to 36-37°C.

Image registration

Structural MRI image preprocessing was performed using the AFNI software package version AFNI_24.2.03 (93). Briefly, magnetization transfer (MT) images for each rat were first deobliqued, spatially oriented, and translated to have spatial overlap with the Waxholm Space reference template (WHS) (71). This space was selected due to its alignment with gold-standard histological rat brain atlases (94, 95) and the atlas's parcellation granularity (N=222 regions). The @animal_warper command (96) was then used to nonlinearly align all MT images to the WHS template. Because some input datasets were notably smaller than the WHS standard template, the -init_scale option was added and used to increase the search space of the registration algorithm, scaled to the relative size ratio of the input scan to the template. Quality control image outputs for each scan (produced by @animal_warper) were then manually reviewed; for any images that were not successfully registered, @animal_warper was run again with the -init_scale parameter altered to better approximate the size ratio. All image registration scripts are available with this publication.

Magnetization transfer ratio (MTR) calculation

MTR was calculated on a per-voxel basis for each scan in native space. First, native scans were scaled according to the receiver gain (RG) parameter used in the scan acquisition protocols (**Supporting Information**). The scaled MT and PD scans in native space were then used to calculate MTR according to

this equation: (PD - MT) / PD. Both steps were executed using 3dcalc in AFNI (93).

Manual evaluation of MTR data quality resulted in the exclusion of 7 scans, typically because of motion artifacts and particularly at the earlier timepoints. Example MT images and their quality control images are shown in **Figure S14**. The analyzable MRI datasets available following preprocessing and quality control of the two cohorts are summarized in **Table S1**. In the normative developmental cohort, a quality control check of the MTR data revealed that, as expected, MTR increased in early development (PND 20 to PND 35) across most cortical systems (excepting the motor cortex) and animals and tended to stay elevated into mid-adulthood (PND 230; **Fig S15A** and **Fig S15B**).

Morphometric Inverse Divergence (MIND) network calculation

MIND networks estimate structural similarity from MRI data (6). Briefly, cortical regions are represented by a distribution of structural MRI features sampled at many points within the region, in this case, at each voxel. The MIND similarity between each pair of regions is then calculated using the Kullback-Leibler (KL) divergence between their feature distributions.

Input data generation: Each MTR image was aligned with the WHS atlas in the native space of the respective MT scan (the scan with the highest contrast), so that each voxel in the MTR scan was labeled with a region of interest based on voxel assignment output from the registration pipeline. For each scan, a two-column CSV was generated, in which the first column “Label” was the region of interest, and the second column (“MTR”) was the value for the corresponding voxel in the MTR scan. For cortical MIND calculation, the input CSV was filtered to contain only voxels belonging to regions under the “Cerebral cortex” hierarchical level of the WHS atlas (which excludes olfactory bulb regions).

MIND network construction: MIND networks were constructed for each scan by calculating the KL divergence between pairwise combinations of regional MTR profiles using the MIND toolkit (https://github.com/isebenius/MIND). The MIND algorithm used can be sensitive to the number of datapoints compared. To balance this, we estimated KL divergence for each pair of regions by estimating the same number of samples (5000) from each region, regardless of its size.

MIND network phenotypes: Edge weight and nodal strength (or weighted degree) were considered as features of interest for downstream analyses. Edge weights were calculated as 1/(1 + KL), per the MIND toolkit. Nodal strength was calculated as the sum of all edge weights for a given region.

Edge distance calculation

The midline of the WHS atlas was determined using the AFNI function 3dcalc to separate the left and right hemispheres. To approximate the center of each WHS region of interest, the AFNI function 3dCM -Icent (93) was then used. The Euclidean distance between pairwise regional centers was then calculated as their edge length.

Rat atlas mapping

We mapped the WHS atlas into Brain Maps 4.0 (BM4) atlas space (95), Zilles atlas space (97), and Allen Mouse Brain Atlas space (AMBA) (98) to compare the MIND similarity network to cortical tract-tracing data (4, 48), cortical type (76), and mouse spatial transcriptomic expression (46), respectively. We did so first by aligning cortical regions based on nomenclature. However, not all regions maintained consistent nomenclature across atlases, so we also visually inspected anatomical alignment of regions using the WHS EBRAINS online resource (https://www.ebrains.eu/tools/rat-brain), BM4 atlas maps (https://sites.google.com/view/the-neurome-project/brain-maps), Zilles atlas cortical maps in stereotaxic coordinates (available for download at https://link.springer.com/book/10.1007/978-3-642-70573-1), and AMBA online interactive atlas viewer (http://atlas.brain-map.org/atlas?atlas=1). Briefly, we identified the position of each region in the reference (BM4, Zilles, or AMBA) atlas maps, then panned through the WHS atlas using the EBRAINS tool to approximate the same coronal slice and identify what region most closely aligned with the reference anatomical position. We also considered relative positioning of surrounding regions to determine this alignment. All atlas mappings are provided as resources in **Tables S4A-C**.

In this work, the BM4 atlas was used as the reference space for the tract-tracing comparison, the Zilles atlas was used as the reference space for the cortical type comparison, and the AMBA atlas provided

reference space for the mouse transcriptomics comparison. If multiple WHS atlas subdivisions comprised a single reference atlas region, the median across these subdivisions was taken as the MIND edge weight for that region.

Tract-tracing Jaccard index calculation

To convert the cortical tract-tracing matrix (4, 48) into a similarity network, the Jaccard index between each pairwise combination of regions was calculated. The set for a given region *a* was defined as the ordinal tract-tracing weight with each other region. The Jaccard index *J* between two regions *a, b* was then calculated as the intersection of their sets divided by the union as follows:

Equation 1

$$J_{ab} = \frac{|a \cap b|}{|a \cup b|}$$

Cortex type network thresholding

WHS cortical regions were categorized by their cortical type using the data presented in (76) and grouped according to whether they are part of the archicortical allocortex or mesocortex (agranular or dysgranular subdivisions). Paleocortical and eulaminate regions were excluded from this analysis due to the very small number of constituent regions defined by the atlas. Each MIND edge was then defined as 'intra-class' or 'inter-class' based on whether both regions were part of the same cortex type or not, respectively. To assess the extent to which top-weighted MIND edges consisted of two regions within the same cortex type, the normative MIND network was thresholded across densities (comprising 0-10% of top-weighted edges), and the percentage of intra-class edges was calculated.

Statistical modeling

Null network generation: Ten thousand null networks were generated to assess whether normative MIND network alignment with tract-tracing similarity and cortical type were greater than would be expected by chance. To do so, all MIND network edges were classified into three evenly sized bins based on distance: proximal, intermediate, and distal (**Fig S6**). Edge weights within each bin were then reshuffled to generate a null network that preserved distance structure. The tract-tracing and cortical type analyses were repeated for each null network to generate a null distribution for comparison of each analysis.

Developmental change: Changes that occurred in edge weight (*w*) and nodal strength (*s*) during normative development (Δw_{dev}; Δs_{dev}) and aging (Δw_{age}; Δs_{age}) were quantified by calculating the linear gradient or slope of age-related change in each period. Early development was defined as PND 20 to PND 35, as the highest proportion of change occurred here, and aging was defined as PND 63 to PND 230. For each region, a linear mixed effects model was fit with the normalized strength as the dependent variable, continuous age and total brain volume as fixed effects, and each individual rat as a random effect:

Equation 2A

$$\textit{normalized strength} \sim \boldsymbol{\beta_1}\ \textit{age} + \beta_2\ \textit{TBV} + (1 \mid \textit{subject})$$

Edge-level analyses were run using coarse-grained systems labels for interpretability. In this case, ROI-level edges were also included as a random effect:

Equation 2B

$$\textit{normalized weight} \sim \boldsymbol{\beta_1}\ \textit{age} + \beta_2\ \textit{TBV} + (1 \mid \textit{subject}) + (1 \mid \textit{ROI edge})$$

The coefficient for age, β_1, was estimated as the slope for that region within the given period. The effect size (Δw; Δs) was used to plot and compare between early development and aging epochs.

RMS-control effect size: Case-control analysis at PND 63 was used to identify changes that occurred in response to RMS and were measurable in young adulthood. For each region, the following model was used:

Equation 3A

$$normalized\ strength \sim \boldsymbol{\beta_1}\ group + \beta_2\ sex + \beta_3\ age + \beta_4\ TBV$$

As with development, case-control edge effects were determined at the systems-level, with ROI-level edges included as a random effect:

Equation 3B

$$normalized\ weight \sim \boldsymbol{\beta_1}\ group + \beta_2\ sex + \beta_3\ age + \beta_4\ TBV + (1 \mid ROI\ edge)$$

The effect size associated with the group term was estimated as the actual case-control effect size for a given region or edge. Then, for each region and edge, 1000 permutations were run in which the group label was randomly sampled, and the case-control effect size was estimated under the null hypothesis. The *Z*-score for each actual effect size in this permutation distribution was calculated; any region with absolute value *Z*-score > 1.96 (*P*=0.05) was considered significant.

Relating developmental changes and case-control stress effects: To characterize the relationship between RMS case-control effects and normative developmental changes, Pearson's correlation was run on Δw_{dev} and Δw_{age} vs edge-level PND 63 case-control effect size. To assess the extent to which the strength of this relationship was greater than expected under the null hypothesis, 10000 permutations were run, in which the edge assignment of RMS effect size was randomly resampled and again correlated with Δw_{dev} and Δw_{age}. The *Z*-score of the actual Pearson's correlation was determined, and the *P*-value was calculated as 1 - (proportion of permuted correlations that were smaller than the observed correlation).

All code for data preprocessing, data analysis, and figure generation is available at https://github.com/rlsmith1/rat_MRI_similarity_networks.

ACKNOWLEDGEMENTS
R.L.S is a PhD candidate in the NIH Oxford-Cambridge Scholars Program. R.L.S., F.J.M., and A.R. are supported by the Intramural Research Program of the National Institute of Mental Health (ZIAMH002843). L.D. and E.G.D. were supported by the Gates Cambridge Scholarship. P.E.V. was supported by MQ: Transforming Mental Health (MQF17_24). P.A.T. and D.R.G. were supported by the NIMH Intramural Research Program (ZICMH002888) of the NIH/HHS, USA. This work received computational support from the NIP HPC Biowulf cluster (http://hpc.nih.gov) and from the mental health theme of the National Institute of Health Research (NIHR) Cambridge Biomedical Research Center. All research from the Department of Psychiatry at the University of Cambridge is made possible by the NIHR Cambridge Biomedical Research Centre and the NIHR East of England Applied Research Centre. The views expressed are those of the author(s) and not necessarily those of the NHS, the NIHR or the Department of Health.

Competing interests: E.T.B has consulted for SR One, GSK, Sosei Heptares, Boehringer Ingelheim, Novartis, and Monument Therapeutics.

REFERENCES

1. D. S. Bassett, O. Sporns, Network neuroscience. *Nat. Neurosci.* **20**, 353–364 (2017).

2. V. Bazinet, J. Y. Hansen, B. Misic, Towards a biologically annotated brain connectome. *Nat. Rev. Neurosci.* 1–14 (2023).

3. I. Sebenius, *et al.*, Structural MRI of brain similarity networks. *Nat. Rev. Neurosci.* 1–18 (2024).

4. L. W. Swanson, J. D. Hahn, O. Sporns, Neural network architecture of a mammalian brain. *Proc. Natl. Acad. Sci. U. S. A.* **121**, e2413422121 (2024).

5. J. Seidlitz, *et al.*, Morphometric Similarity Networks Detect Microscale Cortical Organization and Predict Inter-Individual Cognitive Variation. *Neuron* **97**, 231-247.e7 (2018).

6. I. Sebenius, *et al.*, Robust estimation of cortical similarity networks from brain MRI. *Nat. Neurosci.* **26**, 1461–1471 (2023).

7. W. Li, *et al.*, Construction of individual morphological brain networks with multiple morphometric features. *Front. Neuroanat.* **11**, 34 (2017).

8. V. Bazinet, *et al.*, Assortative mixing in micro-architecturally annotated brain connectomes. *Nat. Commun.* **14**, 2850 (2023).

9. M. Á. García-Cabezas, B. Zikopoulos, H. Barbas, The Structural Model: a theory linking connections, plasticity, pathology, development and evolution of the cerebral cortex. *Brain Struct. Funct.* **224**, 985–1008 (2019).

10. D. Fenchel, *et al.*, Development of microstructural and morphological cortical profiles in the neonatal brain. *Cereb. Cortex* **30**, 5767–5779 (2020).

11. X. Wu, *et al.*, Morphometric dis-similarity between cortical and subcortical areas underlies cognitive function and psychiatric symptomatology: a preadolescence study from ABCD. *Mol. Psychiatry* **28**, 1146–1158 (2023).

12. J. Ruan, *et al.*, Single-subject cortical morphological brain networks across the adult lifespan. *Hum. Brain Mapp.* **44**, 5429–5449 (2023).

13. Y. Shigemoto, *et al.*, Age and sex-related effects on single-subject gray matter networks in healthy participants. *J. Pers. Med.* **13**, 419 (2023).

14. Y. Wang, *et al.*, Age-related differences of cortical topology across the adult lifespan: Evidence from a multisite MRI study with 1427 individuals. *J. Magn. Reson. Imaging* **57**, 434–443 (2023).

15. L. Dorfschmidt, *et al.*, Human adolescent brain similarity development is different for paralimbic versus neocortical zones. *Proc. Natl. Acad. Sci. U. S. A.* **121**, e2314074121 (2024).

16. N. González-García, *et al.*, Resilient functioning is associated with altered structural brain network topology in adolescents exposed to childhood adversity. *Dev. Psychopathol.* **35**, 2253–2263 (2023).

17. T. Tian, *et al.*, Effects of childhood trauma experience and BDNF Val66Met polymorphism on brain plasticity relate to emotion regulation. *Behav. Brain Res.* **398**, 112949 (2021).

18. Y. Xiao, *et al.*, Transcriptional signal and cell specificity of genes related to cortical structural differences of post-traumatic stress disorder. *J. Psychiatr. Res.* **160**, 28–37 (2023).

19. X. Liu, *et al.*, Brain structure and functional connectivity linking childhood cumulative trauma to COVID-19 vicarious traumatization. *J. Child Psychol. Psychiatry* (2024). https://doi.org/10.1111/jcpp.13989.

20. M. D. Hettwer, *et al.*, Longitudinal variation in resilient psychosocial functioning is associated with ongoing cortical myelination and functional reorganization during adolescence. *Nat. Commun.* **15**, 6283 (2024).

21. H. Cao, *et al.*, The alteration of cortical microstructure similarity in drug-resistant epilepsy correlated with mTOR pathway genes. *EBioMedicine* **97**, 104847 (2023).

22. P. Homan, *et al.*, Structural similarity networks predict clinical outcome in early-phase psychosis. *Neuropsychopharmacology* **44**, 915–922 (2019).

23. X. Li, *et al.*, Altered topological characteristics of morphological brain network relate to language impairment in high genetic risk subjects and schizophrenia patients. *Schizophr. Res.* **208**, 338–343 (2019).

24. A. Lisowska, I. Rekik, Joint pairing and structured mapping of convolutional brain morphological multiplexes for early dementia diagnosis. *Brain Connect.* **9**, 22–36 (2019).

25. S. E. Morgan, *et al.*, Cortical patterning of abnormal morphometric similarity in psychosis is associated with brain expression of schizophrenia-related genes. *Proc. Natl. Acad. Sci. U. S. A.* **116**, 9604–9609 (2019).

26. I. Mahjoub, M. A. Mahjoub, I. Rekik, Alzheimer's Disease Neuroimaging Initiative, Brain multiplexes reveal morphological connectional biomarkers fingerprinting late brain dementia states. *Sci. Rep.* **8**, 4103 (2018).

27. L. Vermunt, *et al.*, Single-subject grey matter network trajectories over the disease course of autosomal dominant Alzheimer's disease. *Brain Commun.* **2**, fcaa102 (2020).

28. W. Zhang, *et al.*, Brain gray matter network organization in psychotic disorders. *Neuropsychopharmacology* **45**, 666–674 (2020).

29. J. Seidlitz, *et al.*, Transcriptomic and cellular decoding of regional brain vulnerability to neurogenetic disorders. *Nat. Commun.* **11**, 3358 (2020).

30. B. Ellenbroek, J. Youn, Rodent models in neuroscience research: is it a rat race? *Dis. Model. Mech.* **9**, 1079–1087 (2016).

31. E. C. Bryda, The Mighty Mouse: the impact of rodents on advances in biomedical research. *Mo. Med.* **110**, 207–211 (2013).

32. M. Pagani, A. Bifone, A. Gozzi, Structural covariance networks in the mouse brain. *Neuroimage* **129**, 55–63 (2016).

33. F. Mandino, *et al.*, A triple-network organization for the mouse brain. *Mol. Psychiatry* **27**, 865–872 (2022).

34. G. Allan Johnson, *et al.*, Whole mouse brain connectomics. *J. Comp. Neurol.* **527**, 2146–2157 (2019).

35. J. M. Huntenburg, L. Y. Yeow, F. Mandino, J. Grandjean, Gradients of functional connectivity in the mouse cortex reflect neocortical evolution. *Neuroimage* **225**, 117528 (2021).

36. L. Coletta, *et al.*, Network structure of the mouse brain connectome with voxel resolution. *Sci. Adv.* **6**, eabb7187 (2020).

37. J. M. Stafford, *et al.*, Large-scale topology and the default mode network in the mouse connectome. *Proc. Natl. Acad. Sci. U. S. A.* **111**, 18745–18750 (2014).

38. J. Bogado Lopes, *et al.*, Individual behavioral trajectories shape whole-brain connectivity in mice. *Elife* **12** (2023).

39. D. Benozzo, *et al.*, Macroscale coupling between structural and effective connectivity in the mouse brain. *Sci. Rep.* **14**, 3142 (2024).

40. F. S. Mueller, *et al.*, Behavioral, neuroanatomical, and molecular correlates of resilience and susceptibility to maternal immune activation. *Mol. Psychiatry* **26**, 396–410 (2021).

41. M. R. Bruce, *et al.*, Sexually dimorphic neuroanatomical differences relate to ASD-relevant behavioral outcomes in a maternal autoantibody mouse model. *Mol. Psychiatry* **26**, 7530–7537 (2021).

42. M. Rubinov, R. J. Ypma, C. Watson, E. T. Bullmore, Wiring cost and topological participation of the mouse brain connectome. *Proceedings of the National Academy of Sciences* **112**, 10032–10037 (2015).

43. S. W. Oh, *et al.*, A mesoscale connectome of the mouse brain. *Nature* **508**, 207–214 (2014).

44. B. D. Fulcher, A. Fornito, A transcriptional signature of hub connectivity in the mouse connectome. *Proc. Natl. Acad. Sci. U. S. A.* **113**, 1435–1440 (2016).

45. B. D. Fulcher, J. D. Murray, V. Zerbi, X.-J. Wang, Multimodal gradients across mouse cortex. *Proc. Natl. Acad. Sci. U. S. A.* **116**, 4689–4695 (2019).

46. Z. Yao, *et al.*, A high-resolution transcriptomic and spatial atlas of cell types in the whole mouse brain. *Nature* **624**, 317–332 (2023).

47. MICrONS Consortium, *et al.*, Functional connectomics spanning multiple areas of mouse visual cortex. *bioRxiv* 2021.07.28.454025 (2021).

48. L. W. Swanson, J. D. Hahn, O. Sporns, Organizing principles for the cerebral cortex network of commissural and association connections. *Proceedings of the National Academy of Sciences* **114**, E9692–E9701 (2017).

49. L. W. Swanson, O. Sporns, J. D. Hahn, The network architecture of rat intrinsic interbrain (diencephalic) macroconnections. *Proc. Natl. Acad. Sci. U. S. A.* **116**, 26991–27000 (2019).

50. L. W. Swanson, J. D. Hahn, O. Sporns, Structure–function subsystem model and computational lesions of the central nervous system's rostral sector (forebrain and midbrain). *Proceedings of the National Academy of Sciences* **119**, e2210931119 (2022).

51. L. W. Swanson, J. D. Hahn, O. Sporns, Structure–function subsystem models of female and male forebrain networks integrating cognition, affect, behavior, and bodily functions. *Proceedings of the National Academy of Sciences* **117**, 31470–31481 (2020).

52. L. W. Swanson, J. D. Hahn, O. Sporns, Network architecture of intrinsic connectivity in a mammalian spinal cord (the central nervous system's caudal sector). *Proc. Natl. Acad. Sci. U. S. A.* **121**, e2320953121 (2024).

53. E. Bullmore, O. Sporns, Complex brain networks: graph theoretical analysis of structural and functional systems. *Nat. Rev. Neurosci.* **10**, 186–198 (2009).

54. K. Schmierer, F. Scaravilli, D. R. Altmann, G. J. Barker, D. H. Miller, Magnetization transfer ratio and myelin in postmortem multiple sclerosis brain. *Ann. Neurol.* **56**, 407–415 (2004).

55. L. Turati, *et al.*, In vivo quantitative magnetization transfer imaging correlates with histology during de- and remyelination in cuprizone-treated mice: QUANTITATIVE MAGNETIZATION TRANSFER IMAGING IN CUPRIZONE-TREATED MICE. *NMR Biomed.* **28**, 327–337 (2015).

56. M. Mancini, *et al.*, An interactive meta-analysis of MRI biomarkers of myelin. *Elife* **9** (2020).

57. N. Downes, P. Mullins, The development of myelin in the brain of the juvenile rat. *Toxicol. Pathol.* **42**, 913–922 (2014).

58. K. Hamano, *et al.*, A quantitative study of the progress of myelination in the rat central nervous system, using the immunohistochemical method for proteolipid protein. *Brain Res. Dev. Brain Res.* **108**, 287–293 (1998).

59. L. Mengler, *et al.*, Brain maturation of the adolescent rat cortex and striatum: changes in volume and myelination. *Neuroimage* **84**, 35–44 (2014).

60. W. Han, Y. Pan, Z. Han, L. Cheng, L. Jiang, Advanced maternal age impairs myelination in offspring rats. *Front. Pediatr.* **10**, 850213 (2022).

61. K. L. P. Long, *et al.*, Regional gray matter oligodendrocyte- and myelin-related measures are associated with differential susceptibility to stress-induced behavior in rats and humans. *Transl. Psychiatry* **11**, 1–15 (2021).

62. M. R. Krigman, E. L. Hogan, Undernutrition in the developing rat: effect upon myelination. *Brain Res.* **107**, 239–255 (1976).

63. J. M. Breton, *et al.*, Juvenile exposure to acute traumatic stress leads to long-lasting alterations in grey matter myelination in adult female but not male rats. *Neurobiol. Stress* **14**, 100319 (2021).

64. R. A. Sarabdjitsingh, M. Loi, M. Joëls, R. M. Dijkhuizen, A. van der Toorn, Early life stress-induced alterations in rat brain structures measured with high resolution MRI. *PLoS One* **12**, e0185061 (2017).

65. N. Oldham Green, J. Maniam, J. Riese, M. J. Morris, I. Voineagu, Transcriptomic signature of early life stress in male rat prefrontal cortex. *Neurobiol Stress* **14**, 100316 (2021).

66. M. Abraham, J. Peterburs, A. Mundorf, Oligodendrocytes matter: a review of animal studies on early adversity. *J. Neural Transm. (Vienna)* **130**, 1177–1185 (2023).

67. N. H. Bass, M. G. Netsky, E. Young, Effect of neonatal malnutrition on developing cerebrum. II. Microchemical and histologic study of myelin formation in the rat. *Arch. Neurol.* **23**, 303–313 (1970).

68. Bai L. S., Kinosada Y., Okuda Y., Ning M., Nakagawa T., Changes of magnetization transfer ratio according to rat brain development. *Nihon Igaku Hoshasen Gakkai Zasshi* **56**, 955–960 (1996).

69. J. D. Hahn, *et al.*, An open access mouse brain flatmap and upgraded rat and human brain flatmaps based on current reference atlases. *J. Comp. Neurol.* **529**, 576–594 (2021).

70. J. D. Hahn, C. Duckworth, A brain flatmap data visualization tool for mouse, rat, and human. *J. Comp. Neurol.* **531**, 1008–1016 (2023).

71. H. Kleven, *et al.*, Waxholm Space atlas of the rat brain: a 3D atlas supporting data analysis and integration. *Nat. Methods* **20**, 1822–1829 (2023).

72. A. Fornito, A. Zalesky, E. T. Bullmore, Eds., “Chapter 5 - Centrality and Hubs” in *Fundamentals of Brain Network Analysis*, (Academic Press, 2016), pp. 137–161.

73. A. Fornito, A. Zalesky, E. T. Bullmore, Eds., “Chapter 6 - Components, Cores, and Clubs” in *Fundamentals of Brain Network Analysis*, (Academic Press, 2016), pp. 163–206.

74. E. K. Towlson, P. E. Vértes, S. E. Ahnert, W. R. Schafer, E. T. Bullmore, The rich club of the C. elegans neuronal connectome. *J. Neurosci.* **33**, 6380–6387 (2013).

75. M. P. van den Heuvel, O. Sporns, Rich-club organization of the human connectome. *J. Neurosci.* **31**, 15775–15786 (2011).

76. M. Á. García-Cabezas, J. L. Hacker, B. Zikopoulos, Homology of neocortical areas in rats and primates based on cortical type analysis: an update of the Hypothesis on the Dual Origin of the Neocortex. *Brain Struct. Funct.* **228**, 1069–1093 (2023).

77. R. I. Grossman, J. M. Gomori, K. N. Ramer, F. J. Lexa, M. D. Schnall, Magnetization transfer: theory and clinical applications in neuroradiology. *Radiographics* **14**, 279–290 (1994).

78. G. Douaud, *et al.*, A common brain network links development, aging, and vulnerability to disease. *Proc. Natl. Acad. Sci. U. S. A.* **111**, 17648–17653 (2014).

79. H. Duan, *et al.*, Population clustering of structural brain aging and its association with brain development. (2024).

80. A. M. Fjell, L. McEvoy, D. Holland, A. M. Dale, K. B. Walhovd, What is normal in normal aging? Effects of aging, amyloid and Alzheimer’s disease on the cerebral cortex and the hippocampus. *Prog. Neurobiol.* **117**, 20–40 (2014).

81. B. L. Callaghan, N. Tottenham, The Stress Acceleration Hypothesis: effects of early-life adversity on emotion circuits and behavior. *Current Opinion in Behavioral Sciences* **7**, 76–81 (2016).

82. S. Meier, A. U. Bräuer, B. Heimrich, R. Nitsch, N. E. Savaskan, Myelination in the hippocampus during development and following lesion. *Cell. Mol. Life Sci.* **61**, 1082–1094 (2004).

83. S. M. Ohline, W. C. Abraham, Environmental enrichment effects on synaptic and cellular physiology of hippocampal neurons. *Neuropharmacology* **145**, 3–12 (2019).

84. G. Bramati, P. Stauffer, M. Nigri, D. P. Wolfer, I. Amrein, Environmental enrichment improves hippocampus-dependent spatial learning in female C57BL/6 mice in novel IntelliCage sweet reward-based behavioral tests. *Front. Behav. Neurosci.* **17**, 1256744 (2023).

85. L. R. Stein, K. A. O’Dell, M. Funatsu, C. F. Zorumski, Y. Izumi, Short-term environmental enrichment enhances synaptic plasticity in hippocampal slices from aged rats. *Neuroscience* **329**, 294–305 (2016).

86. J. P. Lerch, *et al.*, Maze training in mice induces MRI-detectable brain shape changes specific to the type of learning. *Neuroimage* **54**, 2086–2095 (2011).

87. K. K. Dayananda, *et al.*, Early life stress impairs synaptic pruning in the developing hippocampus. *Brain Behav. Immun.* **107**, 16–31 (2023).

88. C. J. Zeiss, Comparative milestones in rodent and human postnatal central nervous system

development. *Toxicol. Pathol.* **49**, 1368–1373 (2021).

89. S. M. Kolk, P. Rakic, Development of prefrontal cortex. *Neuropsychopharmacology* **47**, 41–57 (2022).

90. C. Demerens, *et al.*, Induction of myelination in the central nervous system by electrical activity. *Proc. Natl. Acad. Sci. U. S. A.* **93**, 9887–9892 (1996).

91. J. A. Jones, *et al.*, Neurobehavioral Precursors of Compulsive Cocaine Seeking in Dual Frontostriatal Circuits. *Biological Psychiatry Global Open Science* **4**, 194–202 (2024).

92. E. G. Dutcher, *et al.*, Early-life stress biases responding to negative feedback and increases amygdala volume and vulnerability to later-life stress. *Transl. Psychiatry* **13**, 1–11 (2023).

93. R. W. Cox, AFNI: Software for Analysis and Visualization of Functional Magnetic Resonance Neuroimages. *Comput. Biomed. Res.* **29**, 162–173 (1996).

94. G. Paxinos, C. Watson, *The Rat Brain in Stereotaxic Coordinates: Hard Cover Edition* (Elsevier, 2006).

95. L. W. Swanson, Brain maps 4.0—Structure of the rat brain: An open access atlas with global nervous system nomenclature ontology and flatmaps. *J. Comp. Neurol.* **526**, 935–943 (2018).

96. B. Jung, *et al.*, A comprehensive macaque fMRI pipeline and hierarchical atlas. *Neuroimage* **235**, 117997 (2021).

97. K. Zilles, *The Cortex of the Rat: A Stereotaxic Atlas* (Springer Science & Business Media, 2012).

98. E. S. Lein, *et al.*, Genome-wide atlas of gene expression in the adult mouse brain. *Nature* **445**, 168–176 (2007).